MEMS BASED TUNABLE MICROSTRIP PATCH ANTENNA FABRICATED

USING PRINTED CIRCUIT PROCESSING TECHNIQUES

Except where reference is made to the work of others, the work described in this thesis is my own or was done in collaboration with my advisory committee. This thesis does not include proprietary or classified information.

_____

Ronald Edward Jackson, Jr.

Certificate of Approval:

_____	_____
Sadasiva M. Rao Professor Electrical and Computer Engineering	Ramesh Ramadoss, Chair Assistant Professor Electrical and Computer Engineering
_____	_____
Lloyd Riggs Professor Electrical and Computer Engineering	Stephen L. McFarland Dean Graduate School

MEMS BASED TUNABLE MICROSTRIP PATCH ANTENNA FABRICATED USING PRINTED CIRCUIT PROCESSING TECHNIQUES

Ronald Edward Jackson, Jr.

A Thesis

Submitted to

the Graduate Faculty of

Auburn University

in Partial Fulfillment of the

Requirements for the

Degree of

Master of Science

Auburn, Alabama
August 7, 2006

MEMS BASED TUNABLE MICROSTRIP PATCH ANTENNA FABRICATED

USING PRINTED CIRCUIT PROCESSING TECHNIQUES

Ronald Edward Jackson, Jr.

Permission is granted to Auburn University to make copies of this thesis at its discretion, upon request of individuals or institutions at their expense. The author reserves all publication rights.

_____

Signature of Author

_____

Date of Graduation

VITA

Ronald Edward Jackson, Jr., son of Ronald and Margaret Jackson, was born August 3, 1982, in Pensacola, Florida. He graduated summa cum laude from East Hill Christian High School in 2000. He attended Auburn University in Auburn, Alabama for four and half years and graduated with a Bachelor of Wireless Engineering degree in the December of 2004. He was in the first graduating class to be granted the degree. He entered graduate school at Auburn University in January of 2005 to pursue a Masters of Science in Electrical Engineering with a focus in electromagnetics as applied to RF MEMS and Antennas. On May 27, 2006, he married Kristen Michelle Pike, daughter of David and Brenda Pike.

THESIS ABSTRACT

MEMS BASED TUNABLE MICROSTRIP PATCH ANTENNA FABRICATED USING PRINTED CIRCUIT PROCESSING TECHNIQUES

Ronald Edward Jackson, Jr.

Master of Science, August 7, 2006
(B.W.E., Auburn University, 2004)

56 Total Typed Pages

Directed by Ramesh Ramadoss

This thesis presents MEMS-based electrostatically tunable microstrip patch antennas fabricated using printed circuit processing techniques. The microstrip patch is patterned on the top side of a flexible kapton polyimide film, which is suspended above the fixed ground plane using a spacer. The air gap between the microstrip patch and the ground plane is decreased by applying a DC bias voltage between the patch and the ground plane. A decrease in air gap increases the effective permittivity of the antenna resulting in a downward shift in the resonant frequency. The microstrip patch is excited by a slot in the ground plane, which is fed by a coplanar waveguide (CPW) feed line.

Square and circular patch designs are presented in this thesis. A 6 *mm* x 6 *mm* square microstrip patch antenna tunable from 18.34 GHz at 0 V to 17.95 GHz at 268 V (with a tuning range of 390 MHz) is presented. A second design, a 6 *mm* diameter

circular microstrip patch antenna tunable from 16.91 GHz at 0 V to 16.64 GHz at 165 V (with a tuning range of 270 MHz) is also presented.

The important feature of the tunable microstrip patch antenna presented here is that it is suitable for fabrication using proven printed circuit processing techniques such as photolithography, wet, and dry etching techniques. These new tunable microstrip antennas are inexpensive as well as versatile and are suitable for implementation of a large inexpensive tunable reconfigurable RF front end, tunable reflect array, etc..

ACKNOWLEDGEMENTS

The author would like to thank Dr. Ramesh Ramadoss for his patience and guidance during this research. Thanks also goes to Raghav Goteti for his work on this research and helping the author get started. A special thanks to father, Ron, mother, Margaret, and sister, Claire, for their love and support throughout the undergraduate and graduate experience. Very special thanks to my wife, Mrs. Kristen Pike Jackson, for her love and support through the ups and downs of graduate school.

Style Manual or Journal used: Standard Format for Publications per the Graduate School Style Manual

Computer Software used: Microsoft Office Word 2003 SP2

TABLE OF CONTENTS

LIST OF FIGURES xi

LIST OF TABLES xiii

CHAPTER 1 INTRODUCTION 1

CHAPTER 2 DESIGN AND MODELING 3
2.1 Design Equations 3
2.2 RF Modeling 7
2.3 Electromechanical Modeling 8
2.4 Effect of Air Gap on the Resonant Frequency 8
2.5 DC Biasing 11

Chapter 3 SQUARE PATCH ANTENNA 13
3.1 RF Design and Simulation 13
3.2 Experimental Characterization 14
3.2.1 WYKO Profiler 14
3.2.2 Return Loss Measurements 15
3.2.3 Radiation Pattern Measurement 17

CHAPTER 4 CIRCULAR PATCH ANTENNA 19
4.1 RF Design and Simulation 19
4.2 Experimental Characterization 21
4.2.1 WYKO Optical Profiler 21
4.2.2 Return Loss Measurements 24
4.2.3 Radiation Pattern Measurement 25

CHAPTER 5 FABRICATION 29
5.1 Material and Setup 29
5.1.1 Glass Mask Selection 30
5.2 Processing 30
5.2.1 Kapton Top Layer 30
5.2.1.1 Photolithography 31
5.2.1.2 Wet Etching 32
5.2.1.3 Deep Reactive Ion Etching 32
5.2.1.4 Probe Station Resistance Measurement 33
5.2.1.5 Removal of Kapton Film from Wafer 34

5.2.2 RT/Duroid Substrate 34
5.2.3 Cleaning of Kapton and Substrate 34
5.2.4 Annealing 35
5.2.5 Lamination 35

CHAPTER 6 CONCLUSION AND FUTURE WORK 38
6.1 Conclusion 38
6.2 Future Work 38

REFERENCES 40
APPENDIX A 42
A.1 Detailed Fabrication Procedures 42
A.2 Chemical Solutions 43
A.2.1 Nichrome Etchant 43
A.2.2 Post DRIE Aluminum Etchant 43
A.2.3 2% Sulfuric Acid Solution 43
A.3 Chemical Incompatibilities 43

LIST OF FIGURES

Figure 1: Cross section of the suspended microstrip patch design. 4

Figure 2: Top view of the suspended microstrip patch and flexures. 4

Figure 3: Ansoft HFSS model of MEMS tunable antenna. 7

Figure 4: CoventorWare 2005 model of the MEMS tunable antenna. 8

Figure 5: Simulated return loss of the square patch antenna for various gap heights (h_1) [4]....9

Figure 6: Resonance frequency versus air gap height, (h_1) for various kapton thicknesses. (a) Square patch and (b) circular patch....10

Figure 7: Pull down voltage versus air gap height for various kapton thicknesses. (a) Square patch and (b) circular patch....11

Figure 8: Nichrome bias lines used for biasing the suspended patch. 12

Figure 9: Top view of the suspended patch showing kapton flexures and bias lines....14

Figure 10: Cross sectional view of the suspended patch antenna showing various layers....14

Figure 11: 3D profile of the antenna measured using WYKO optical profiler (top left quarter shown) [5]. 15

Figure 12: Return loss measurement setup with bias tee....16

Figure 13: Measured and simulated return loss for the up and down states for the square patch antenna....16

Figure 14: Measured radiation patterns of the frequency switchable patch antenna (a) E plane pattern and (b) H plane pattern....18

Figure 15: Cross sectional view of the suspended patch antenna showing various layers....19

Figure 16: E field distribution plots (a) for circular patch using slot design from square path and (b) circular patch using new slot design. 20

Figure 17: CPW feed line and coupling slot. 21

Figure 18: 2D profile of the circular patch antenna measured using WYKO NT 2000 optical profiler..... 23

Figure 19: Measurement setup used for testing antenna using the HP 8510C VNA..... 24

Figure 20: Measured return loss (S_{11}) for the circular patch for various applied voltages. 25

Figure 21: E and H plane of the circular patch antenna..... 26

Figure 22: Radiation patterns for circular patch antenna for various applied voltages. The simulated pattern is in the up state. (a) E co-polarization (b) E cross polarization (c) H co-polarization (d) H cross polarization..... 27

Figure 23: Radiation patterns for circular patch antenna for various applied voltages compared to the simulation results from the warped model in the up state. (a) E co-polarization (b) E cross polarization (c) H co-polarization (d) H cross polarization. 28

Figure 24: Masks used in photolithography: (a) dummy mask, (b) electrode mask, (c) bias line definition mask, (d) DRIE mask, and (e) CPW mask..... 32

Figure 25: Bonding jig used in lamination. 36

Figure 26: Final sequence of layers for MEMS tunable antenna as on bonding jig..... 37

LIST OF TABLES

Table 4.1: Performance summary of the MEMS based tunable circular patch antenna for various applied voltages..... 25

Chapter 1 INTRODUCTION

Microstrip patch antennas are extensively used in commercial and military communication systems. Advantages of using microstrip patch antennas over conventional antennas are their light weight, low profile and volume, and low cost of fabrication [1]. However, with such great advantages come drawbacks. Microstrip patch antennas are known for having narrow bandwidths and narrow design tolerances.

In its simplest form, a microstrip patch antenna is a radiating patch on the top side of a dielectric substrate with a ground plane on the bottom side of the substrate. It is well known that the resonant frequency of a microstrip patch antenna can be tuned by adjusting the substrate thickness. In the early 1980's, a manually tunable circular microstrip patch antenna was reported by Lee et. al [2]. The tuning was achieved by manually adjusting the air gap between the substrate and the ground plane using a spacer. A tunable microstrip patch antenna increases the usefulness of the design by allowing for a broader range of frequency operation than allowed by traditional microstrip design.

Micro-electromechanical Systems (MEMS) are devices ranging from a few millimeters to a few micrometers in size that can convert electrical, thermal energy, etc. into mechanical movement, and vice versa. In this thesis a MEMS tunable microstrip patch antenna is presented. By applying the MEMS electrostatic movement to the work done by Lee et. al [2], an electrostatically tunable antenna can be constructed.

The microstrip patch is patterned on the top side of the flexible kapton polyimide film, which is suspended above the fixed ground plane using a spacer. The air gap between the patch and the ground plane is decreased by applying a DC bias voltage between the patch and the ground plane. A decrease in the air gap results in a downward shift in the resonant frequency. The microstrip patch is excited by a slot in the ground plane.

Square and circular microstrip patch designs will be presented in this thesis. It will be shown that a MEMS tunable square microstrip patch fabricated on flexible polyimide material yields a tunable range of 390 MHz with bias voltages between 0 V and 268 V, while a tunable circular microstrip patch yields a tunable range of 270 MHz with bias voltages between 0 V and 165 V.

Chapter 2 DESIGN AND MODELING

The MEMS tunable antenna presented in this work consists of three layers: a 30 mil thick RT/Duroid 6002 (ε_r = 2.94, tanδ = 0.001) substrate with ¼ oz of copper cladding, a 2 mil thick flexible kapton E polyimide film (ε_r = 3.1) with 3 μm copper cladding and a 2 mil thick polyflon bonding spacer film. Two areas are important to consider in the design of this device: RF design and electromechanical design. The RF design of the patch antenna was done in a commercially available EM software package, Ansoft HFSS 10 [7], and electromechanical simulations for determining pull down voltages were done in CoventorWare 2005 [7].

2.1 Design Equations

Figure 1 shows the patch of width W defined on the dielectric layer. The dielectric layer has a thickness h_2, permittivity ε_r, and is suspended above the ground plane at a height h_1. There are several fundamental equations considered in the design of square and circular patch antennas [1]. For the square patch design, simple rectangular microstrip patch design equations were used. To accommodate for movement of the MEMS device for tuning, the microstrip patch is suspended above an air gap.

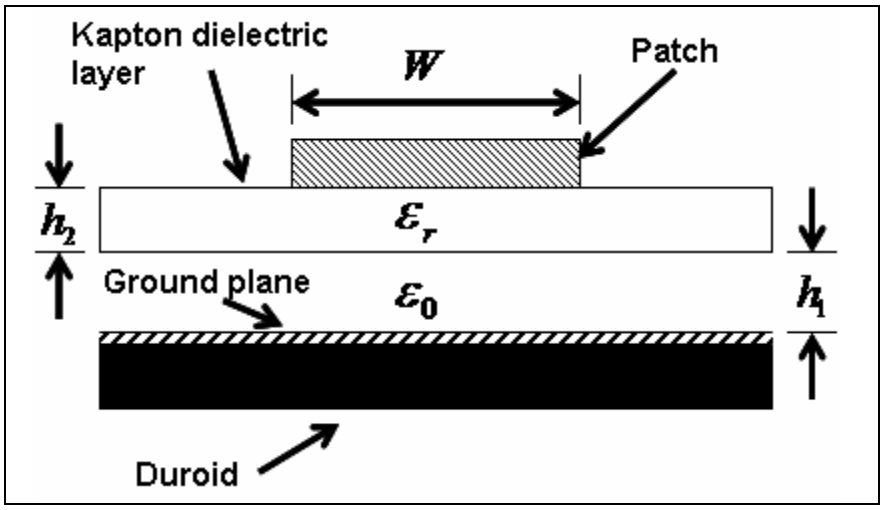

Figure 1: Cross section of the suspended microstrip patch design.

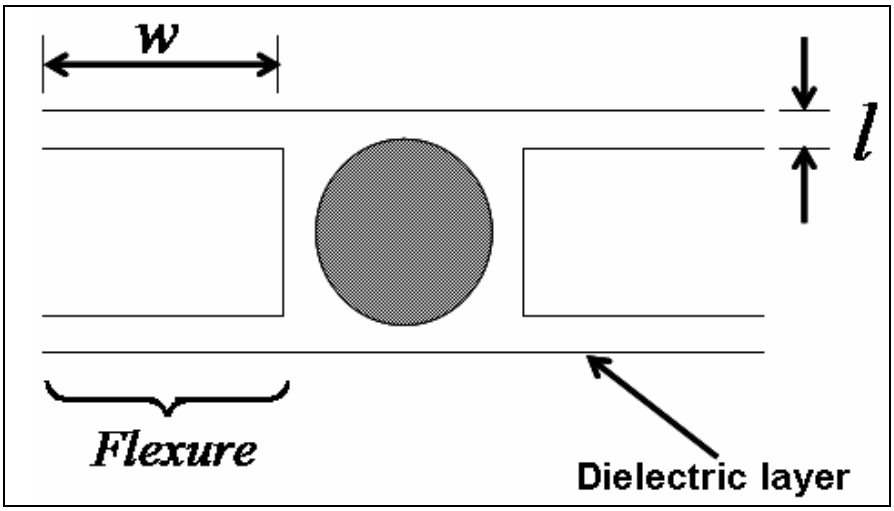

Figure 2: Top view of the suspended microstrip patch and flexures.

The equation for effective dielectric, ε_{eff} of the patch is given by

$$\varepsilon_{eff} = \frac{\varepsilon_r}{\varepsilon_r + \frac{h_2}{h_1 + h_2}(1 - \varepsilon_r)} \tag{1}$$

where ε_r is the dielectric constant and h_2 is the thickness of the kapton dielectric layer. h_1 is the air gap height between the dielectric layer and the ground plane. Effective dielectric can then be used to find the resonant frequency of the antenna by

$$f_0 = \frac{c}{2L\sqrt{\varepsilon_{eff}}} \tag{2}$$

where $c = 300 \times 10^6 m/s$, the velocity of light in free space. Equation (2) will yield the frequency of the up state of the square MEMS device when h_1 is maximum. It should be noted that these equations are simplified approximations of the suspended patch; therefore experimental results should follow the calculated trends but may vary in actual values.

The equations for a circular patch of the same configuration as Figure 1, where the patch radius a is defined as $a = W/2$, are given by Garg, et. al. and provide approximations for characterizing a circular microstrip patch with two dielectrics [1]. Again, it is important to find the effective dielectric constant. In the case of the circular patch, ε_{eff} is given by

$$\varepsilon_{eff} = \frac{\varepsilon_r (h_2 + h_1)}{h_2 + \varepsilon_r h_1}. \tag{3}$$

The effective radius must also be calculated to account for the fringing fields of the circular disk, as shown in (4).

$$a_e = a\sqrt{1 + \frac{2h_2}{\pi a \varepsilon_{eff}}\left(\ln\left(\frac{\pi a}{2h_2}\right) + 1.7726\right)} \tag{4}$$

Both (3) and (4) can be used to calculate the resonant frequency f_{nm}. In this case, mode f_{11} is the mode of interest, therefore from Table 5 on page 320 of [1] it is found that $x_{11} = 1.84118$. The resonant frequency of the circular disk microstrip patch is found to be

$$f_{11} = \frac{(1.84118)c}{2\pi a_e \sqrt{\varepsilon_{eff}}} \tag{5}$$

where $c = 300 \times 10^6 m/s$, the velocity of light in free space.

In order to be able to tune the suspended patch antenna, the air gap must be reduced. In both (1) and (3), it can be seen that when h_1 is maximum, or 50.8 microns, the effective dielectric ε_{eff} is less than ε_r, and when $h_1 = 0$, $\varepsilon_{eff} = \varepsilon_r$. It is therefore possible to tune the resonant frequency of the suspended microstrip patch antenna by changing the air gap h_1. The device is basically a parallel plate electrostatic actuator, where the voltage is applied to the movable suspended patch and the DC ground is connected to the ground plane. The suspended patch antenna is pulled down towards the ground plane due to the electrostatic force of attraction. The voltage required to actuate the antenna is given in [12] by

$$V = \sqrt{\frac{8k(z^3)}{27(\varepsilon_{eff}\varepsilon_0)A}}. \tag{6}$$

Where A is the area of the suspended patch, z is the gap height between the patch and the ground plane, $\varepsilon_0 = 8.845 \times 10^{-12} F/m$. k is the spring constant of the suspended structure given by

$$k = 4Ew\left(\frac{t}{l}\right)^3 \tag{7}$$

where E is the Young's modulus of kapton, w, t, and l are the width, thickness and length of one of the flexures (shown in Figure 2), respectively.

2.2 RF Modeling

The RF performance of the patch antenna was modeled and simulated using Ansoft's HFSS and Agilent's Advanced Design System (ADS) [7][9]. The layers modeled in HFSS were the patch, kapton, CPW and RT/Duroid substrate layers. The moveable flexures were not included in the simulation. To model various tuned states of the device, separate models with different air gap heights were created. The model is shown in Figure 3. The suspended microstrip patch is excited by aperture coupling using a slot in the ground plane. The slot is fed by a 50 Ω CPW feed line shown in Figure 9 for the square design. The dimensions of the 50 Ω CPW feed line were calculated using the Agilent Advanced Design System (ADS) LineCalc tool [9].

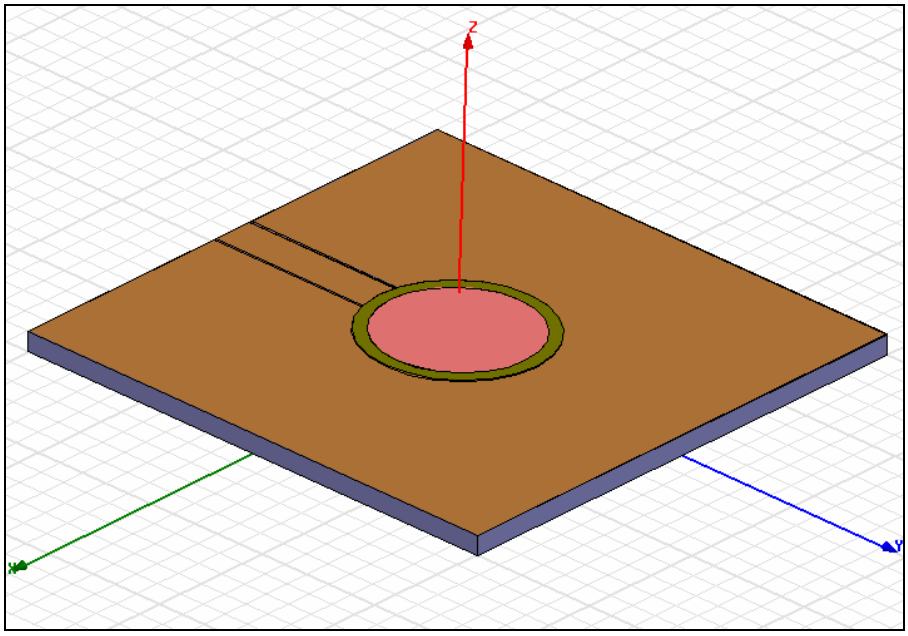

Figure 3: Ansoft HFSS model of the MEMS tunable circular antenna.

2.3 Electromechanical Modeling

Electromechanical modeling was done in ConventorWare 2005, a powerful software package designed for modeling of MEMS devices [7]. CoventorWare can model electrostatic charge for various applied voltages and deflection of moveable components due to force in separate simulation tools called MEMelectro and MEMmech, respectively. A more complex simulation tool called CosolveEM is used for simulating the applied voltage versus deflection characteristics of the suspended patch. The suspended antenna design is basically modeled as a fixed-fixed beam design with flexures, patch and ground plane in CoventorWare (Figure 4).

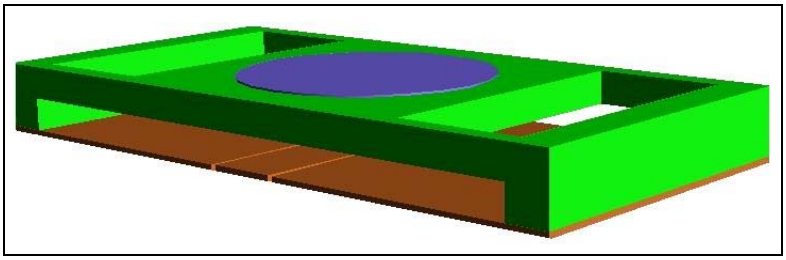

Figure 4: CoventorWare 2005 model of the MEMS tunable antenna.

2.4 Effect of Air Gap on the Resonant Frequency

Electromagnetic simulations of the antenna were performed in ADS Momentum for various air gaps (h_1) using the optimized feed design for slot and CPW for the square design discussed in Chapter 3 . The simulated return loss of the square tunable patch antenna for various air gaps (h_1) is shown in Figure 5. It can be noted that the resonant frequency (f_0) of the antenna decreases as the air gap (h_1) is decreased. As the air gap is decreased, the effective permittivity of the antenna increases. Therefore, the antenna exhibits a downward shift in the resonant frequency [4].

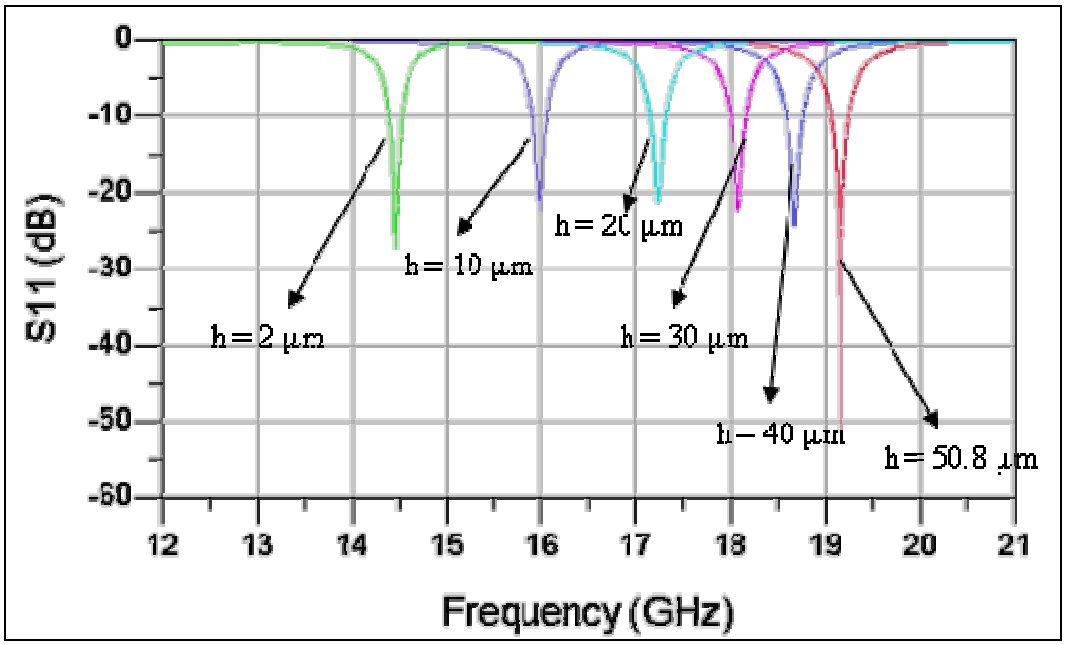

Figure 5: Simulated return loss of the square patch antenna for various gap heights (h_1) [4].

Simulations were also done in Matlab using the equations outlined in section 2.1 to determine the expected tunable range for the antenna. 2 mil as well as 1 mil kapton was used in these calculations. Plots showing the resonant frequency versus gap height, and required pull down voltage versus gap height for both the square and circular design are shown in Figure 6 and Figure 7, respectively.

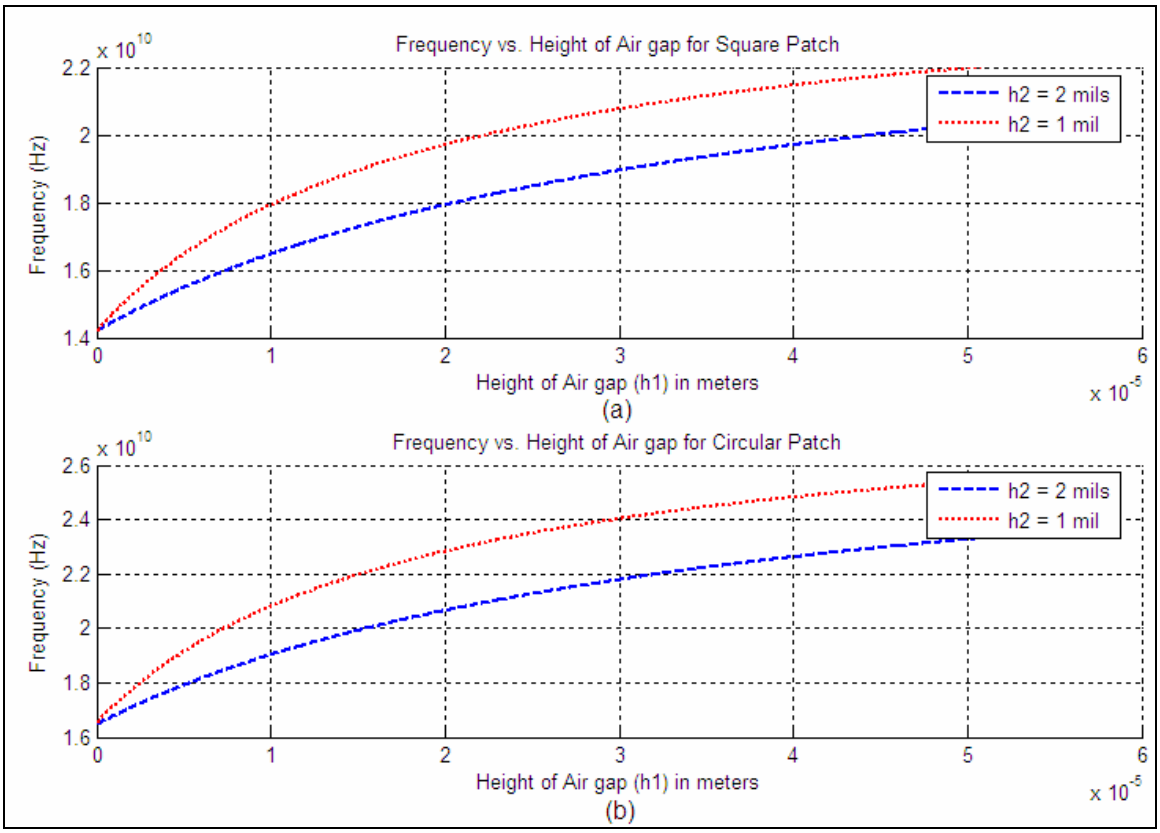

Figure 6: Resonance frequency versus air gap height, **(h_1)** for various kapton thicknesses. (a) Square patch and (b) circular patch.

From Figure 6 it can be seen that the resonant frequency decreases when air gap (h_1) is decreased. Also, it can be noted that a reduced kapton thickness increases the possible tuning range. Similarly, Figure 7 shows that the pull down voltage is proportional to gap height, and also reveals that the thicker kapton film requires a higher pull down voltage.

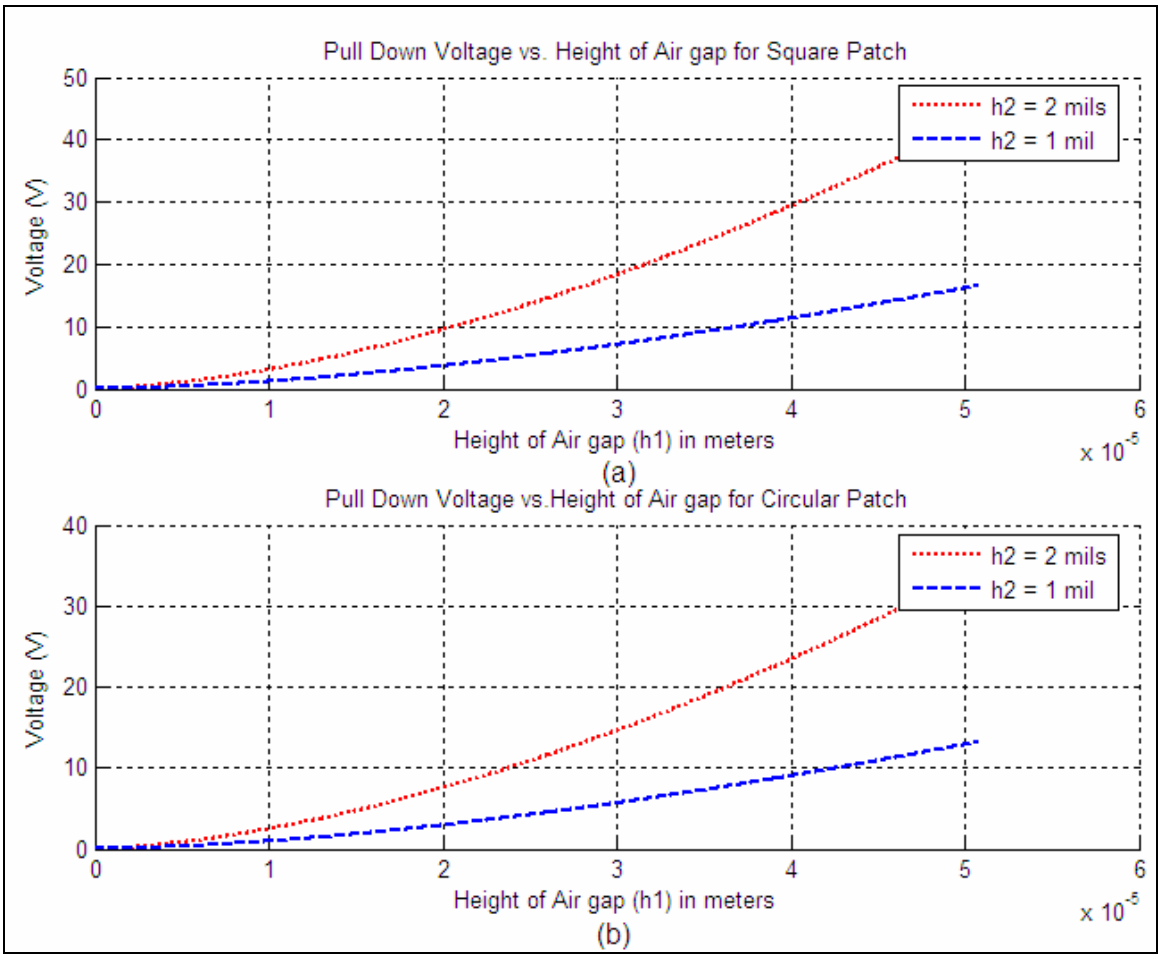

Figure 7: Pull down voltage versus air gap height for various kapton thicknesses. (a) Square patch and (b) circular patch

2.5 DC Biasing

A DC voltage is applied to the patch to induce a potential difference between the patch and the ground plane. The electrostatic forces which result from this potential difference cause the patch to move toward the ground plane, enabling tuning of the resonant frequency. This voltage must be applied to the patch without interfering with the RF characteristics of the patch. A nichrome bias line was designed to connect the patch to an electrode via the flexures (Figure 8). The nichrome provides a resistive connection between the biasing electrode and the patch. The resistive nature of the connection prevents any RF leakage from the patch, preserving the RF characteristics of the antenna,

as well as preventing damage to the DC power supply. The design calls for two lines, one on each flexure closest to the biasing copper electrode, primarily to reduce the chances of bias line breakage during the fabrication process.

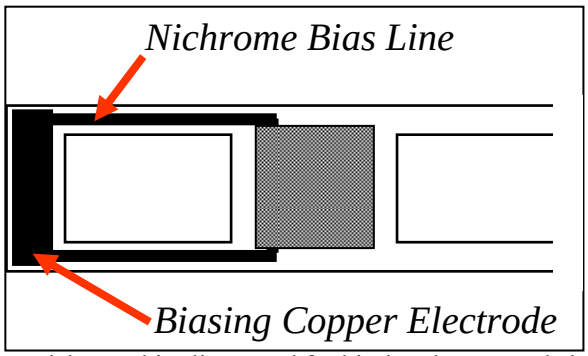

Figure 8: Nichrome bias lines used for biasing the suspended patch.

The nichrome bias lines have a width of 30 microns, length of 10 *mm* and thickness of 100 Å. Equation 8 gives the resistance of one bias line as

$$R = \frac{\rho l}{wt} \tag{8}$$

where $\rho = 1.1 \times 10^{-6}\ \Omega / m$, the resistivity of the nichrome, l, w, t are the length, width and thickness of the line, respectively. This yields a resistance of 36.6 kΩ per line, or a total resistance of 18.3 kΩ.

Chapter 3 SQUARE PATCH ANTENNA[1]

In this chapter, design, simulation and experimental characterization of a square patch antenna are discussed.

3.1 RF Design and Simulation

The tunable square patch antenna is made of a 6 *mm* x 6 *mm* microstrip patch with a resistive nichrome bias line defined on the top side of the kapton film. The copper cladding on the duroid substrate serves as the ground plane of the microstrip patch. The microstrip patch is suspended above the fixed ground plane by mechanical flexures (as shown in Figure 9) machined in kapton film using an excimer laser. The flexure dimensions are: flexure length F_l = 3 *mm* and width F_w = 0.5 *mm*. The microstrip patch is excited by aperture coupling using an inductively coupled slot in the ground plane. The slot is fed by a 50 Ω CPW feed line. The design parameters of the CPW feed line are: center conductor width W_c = 1.627 *mm* and gap dimension W_g = 0.1 *mm*. The length and width of the slot are S_w = 50 μm and S_l = 3.5 *mm*, respectively. Figure 10 shows a cross sectional view of the MEMS tunable antenna. The spacer film introduces an air gap between the kapton film and the ground plane. A DC bias voltage applied between the movable patch and the fixed ground plane decreases the effective air gap due to electrostatic force of attraction between the patch and the ground plane. A decrease in air gap increases the effective permittivity of the antenna resulting in a downward shift in the

[1] Research on the MEMS tunable square microstrip antenna was done jointly with Raghav V. Goteti.

resonant frequency. The substrate, the spacer and the Kapton film are laminated by thermo-compression bonding to obtain the frequency tunable antenna. The fabrication and assembly of the MEMS based tunable antenna are described in Chapter 5 and listed in detail in Appendix A.1.

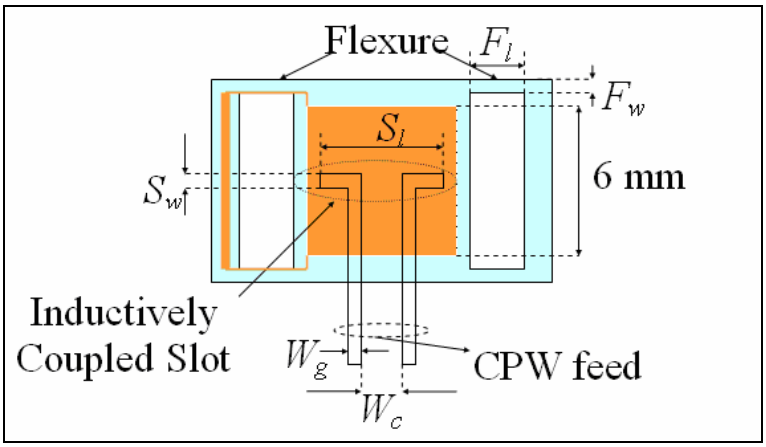

Figure 9: Top view of the suspended patch showing kapton flexures and bias lines.

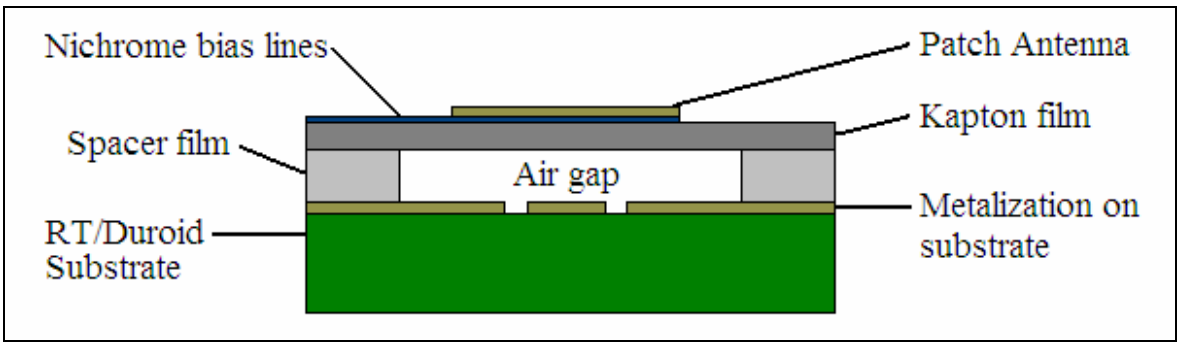

Figure 10: Cross sectional view of the suspended patch antenna showing various layers.

3.2 Experimental Characterization

3.2.1 WYKO Profiler

The profile of the suspended patch antenna was measured using a WYKO NT 2000 optical profiler and is shown in Figure 11. The height of the antenna between the top surface of the kapton and the ground plane was measured to be 110 μm, which is higher than the expected value of 101.6 μm. The air gap is large due to warpage caused by the

thermal expansion mismatch between the patch metallization (copper) and the kapton polyimide film. This warpage occurred during thermo-compression bonding. As a result, the voltage required for changing the resonant frequency of the antenna is higher than expected.

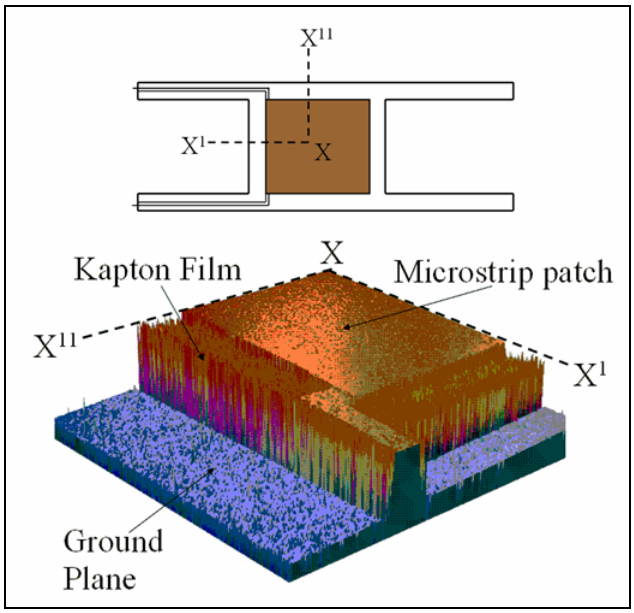

Figure 11: 3D profile of the antenna measured using WYKO optical profiler (top left quarter shown) [5]**.**

3.2.2 Return Loss Measurements

The fabricated antenna was characterized using an HP 8510C Vector Network Analyzer (VNA). DC bias voltage was applied using a bias tee connected at the input port of the antenna. This setup can be seen in Figure 12. The measured return loss of the antenna for applied DC bias voltages of 0 V and 268 V corresponding to the up and down positions, respectively, is shown in Figure 13. In the up-position, the resonant frequency of the antenna is 18.34 GHz. The return loss is 40.6 dB at 18.34 GHz and the bandwidth is about 0.85 GHz for a return loss better than 10 dB.

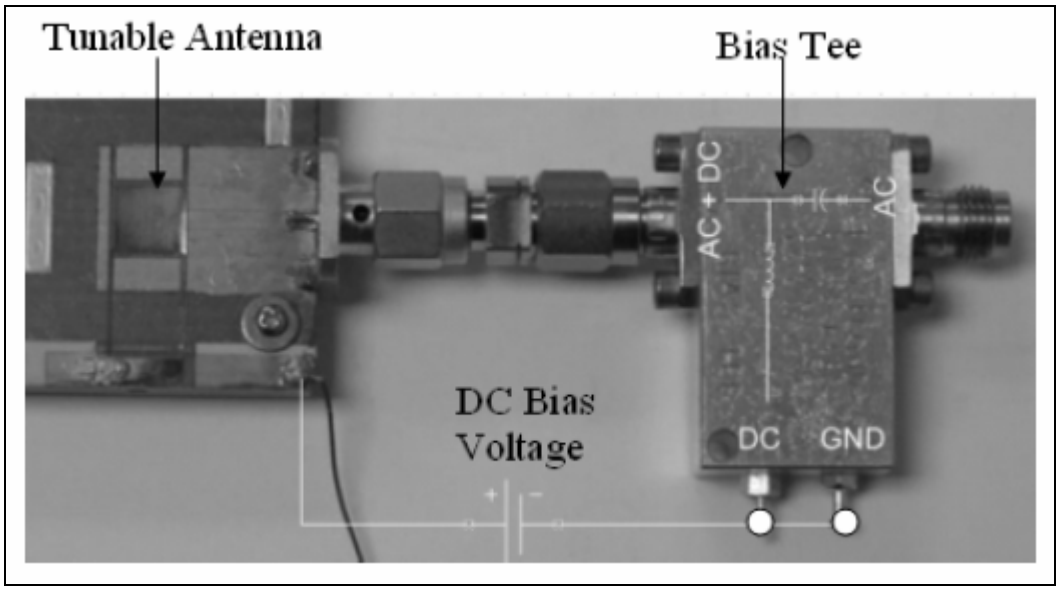

Figure 12: Return loss measurement setup with bias tee.

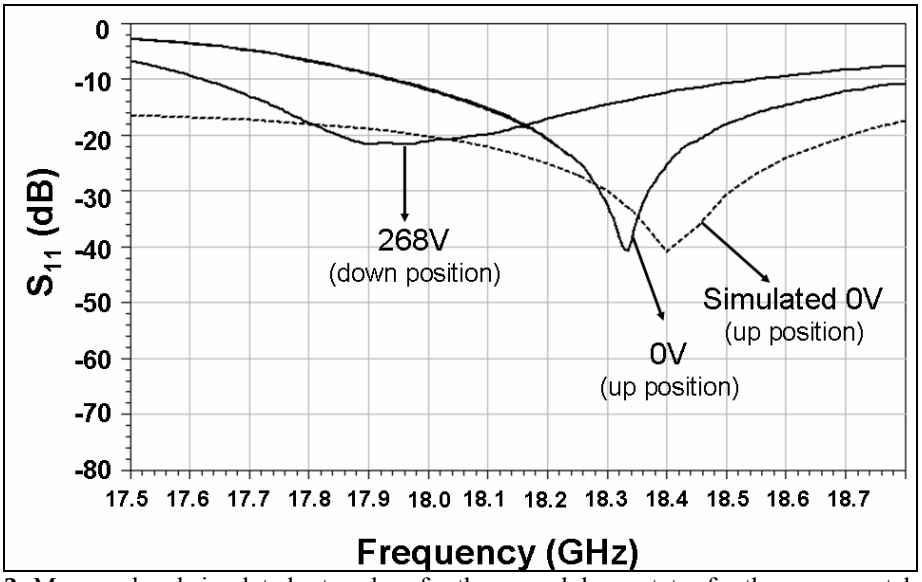

Figure 13: Measured and simulated return loss for the up and down states for the square patch antenna**.**

For the purposes of comparing the measured results with the simulated results, the measured profile of the warped patch antenna in the up position was used to create a 3D model in Ansoft HFSS [7]. The simulated return loss of the warped patch antenna model in the up position corresponding to the zero bias state is also shown in Figure 13. It can be noted that the simulated resonant frequency of the antenna is 18.40 GHz, which is close to the measured resonant frequency 18.34 GHz at 0 V. The slight discrepancy

between the measured and simulated resonant frequency may be attributed to the approximate geometric modeling of the warped antenna in HFSS. As the voltage is increased to the pull down voltage of 268 V, the patch antenna on the kapton film snaps down onto the substrate. At the pull down voltage, the resonant frequency of the antenna is 17.95 GHz. When the voltage is decreased below the pull down voltage the patch antenna releases completely from the substrate at 156 V. The return loss is 20.1 dB at 17.95 GHz and the bandwidth is about 0.95 GHz for a return loss better than 10 dB. This movement reflected band switching rather than precise tuning. Thus, the antenna can be switched from 18.34 GHz at 0 V (up position) to 17.95 GHz at 268 V (down position) with a switching range of 390 MHz. The percentage frequency switching of the antenna is about 2.2%

3.2.3 Radiation Pattern Measurement

The radiation pattern of the antenna for various applied bias voltages was measured using an in-house pattern measurement system. The measured E plane and H plane radiation patterns for V_{dc} = 0 V and 268 V are shown in Figure 14. It can be noted that the overall antenna pattern remains the same for both bias voltages. However, the main beam is tilted due to warpage of the patch which is confirmed by simulated radiation pattern of the warped model. The cross-polarization radiation level is 10 dB below the co-polarization radiation.

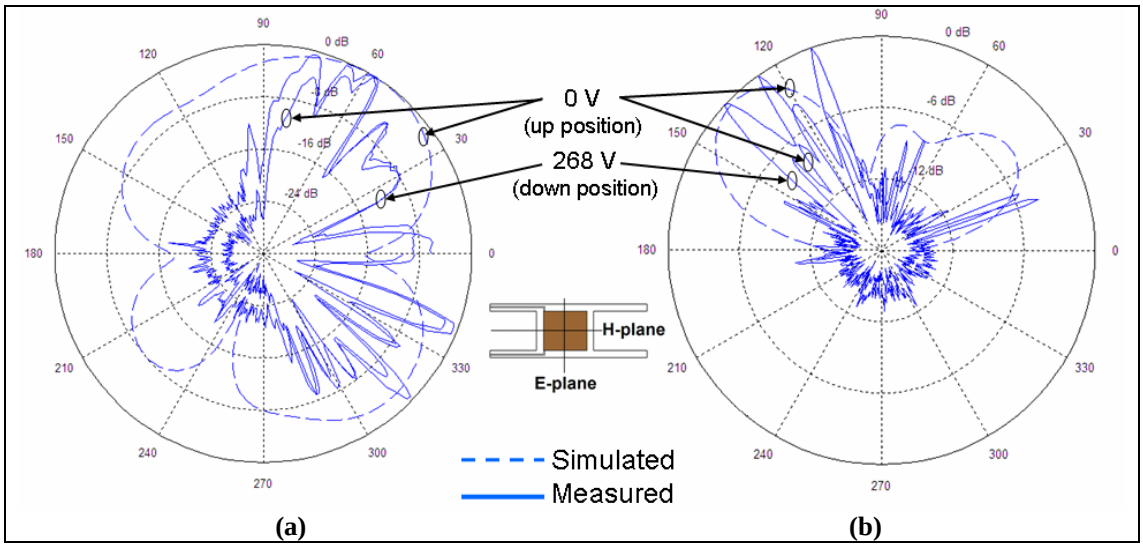

Figure 14: Measured radiation patterns of the frequency switchable patch antenna (a) E plane pattern and (b) H plane pattern

Chapter 4 CIRCULAR PATCH ANTENNA

In this chapter, design, simulation and experimental characterization of a MEMS based tunable circular patch antenna are discussed.

4.1 RF Design and Simulation

Figure 15 shows the cross sectional view of the MEMS tunable circular microstrip patch antenna. In the circular patch design, a 6 *mm* diameter circular microstrip patch is patterned on the top side of the flexible kapton film ($\varepsilon_r = 3.1$). The dimensions of the kapton flexures are the same as that of the square design. The microstrip patch is excited by aperture coupling through a slot in the ground plane. The slot is fed by a 50 Ω CPW feed line shown in Figure 17. The slot and the CPW line were defined on the RT/Duroid 6002 substrate ($\varepsilon_r = 2.94$). The RF performance of the patch antenna was simulated using Ansoft's HFSS.

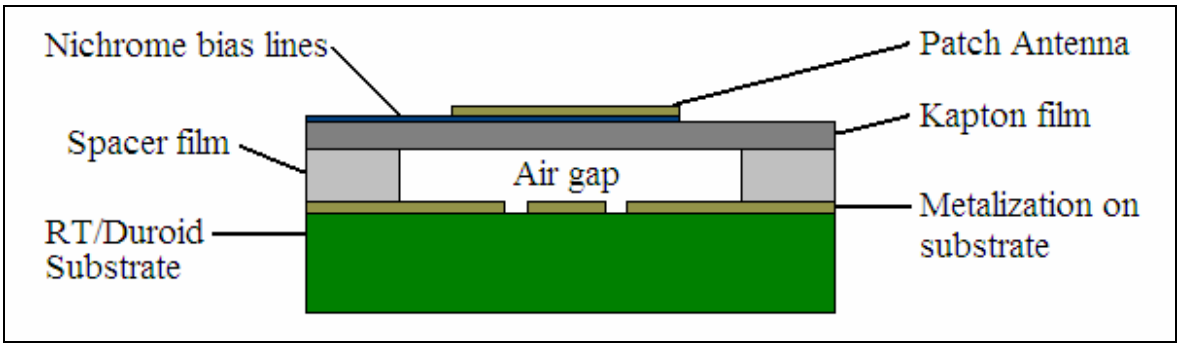

Figure 15: Cross sectional view of the suspended patch antenna showing various layers.

The dimensions of the 50 Ω CPW feed line were calculated using the ADS tool, LineCalc [9]. Calculated dimensions of the CPW were: center conductor width $W_c = 1.652\ mm$ and gap width $W_g = 0.09\ mm$ for frequencies around 16.9 GHz.

It was discovered through simulations in HFSS that the feed and slot design used for the square patch in Chapter 3 yielded an asymmetrical E field for the circular patch design (Figure 16(a)). In the square patch design the coupling slot was located at the end of the CPW feed line and centered below the square patch with $S_1 = 3.5\ mm$ and $S_w = 50\ \mu m$.

Alternative feed designs were simulated until an optimal design was reached. Trent et. al. had done work on slot coupled microstrip antennas in [6]. The feed used by Trent was a capacitive coupled feed. The feed line and slot design used for this device was an adaptation from work done by Trent [6].

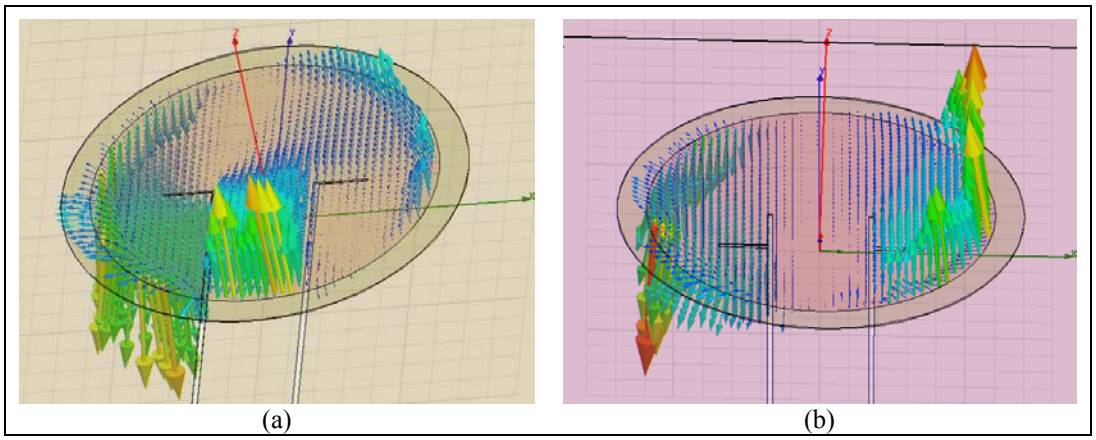

(a) (b)

Figure 16: E field distribution plots (a) for circular patch using slot design from square path and (b) circular patch using new slot design.

In [11] it was reported that it is easier to match specified impedance with an inductive (short) coupling design over a capacitive (open) coupling design. The inductively coupled feed with offset slot was chosen with $L_s = 848\mu m$, $L_A = 890\mu m$, $L_B = 885\mu m$ (Figure 17).

Good matching is achieved with slot widths $S_{WA} = 115\mu m$ and $S_{WB} = 120\mu m$ at 16.91 GHz. Through EM simulation it was determined that the new feed, with input impedance of $48\,\Omega$, provides optimum coupling, yielding a symmetrical E-field on the patch as shown in Figure 16(b).

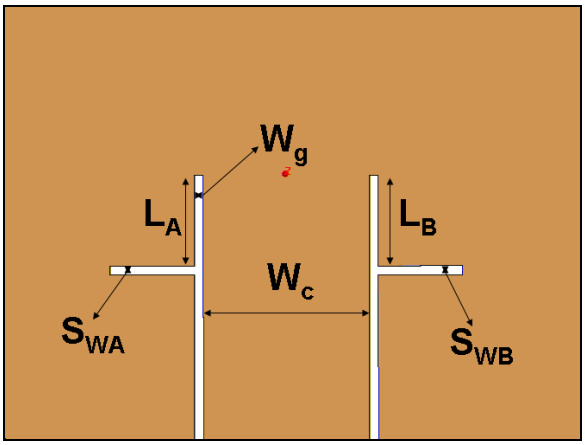

Figure 17: CPW feed line and coupling slot.

4.2 Experimental Characterization

An SMA launcher was soldered to the CPW feed line for RF testing. Three types of measurements were taken to characterize the antenna: profile, return loss, and radiation pattern. The profile of the MEMS device was measured using a WYKO NT 2000 optical profiler. Return losses were measured using an HP 8510C Vector Network Analyzer (VNA). The pattern measurements were taken using a desktop antenna measurement system (DAMS) inside an anechoic chamber. To ensure rigidity of the MEMS devices during testing, the substrate was mounted to a Lucite frame.

4.2.1 WYKO Optical Profiler

The WYKO optical profiler was used to determine the flatness of the MEMS device and the measured profile of the circular patch is shown in Figure 18. For optimal

operation, the patch and moveable flexures must not be warped. It was found that the antenna had warpage of 10 to 15 microns across the surface of the circular patch. The height of the suspended antenna above the ground plane was 90 to 100 microns. During lamination of the final design, spare kapton pieces were placed in the gap to help reduce warpage during bonding. As a result, the warpage of the circular patch is considerably lower than that of the square patch. It is apparent, however, that the thermal coefficient of expansion mismatch between the copper patch (17 ppm) and kapton (16 ppm) is still an issue for the design.

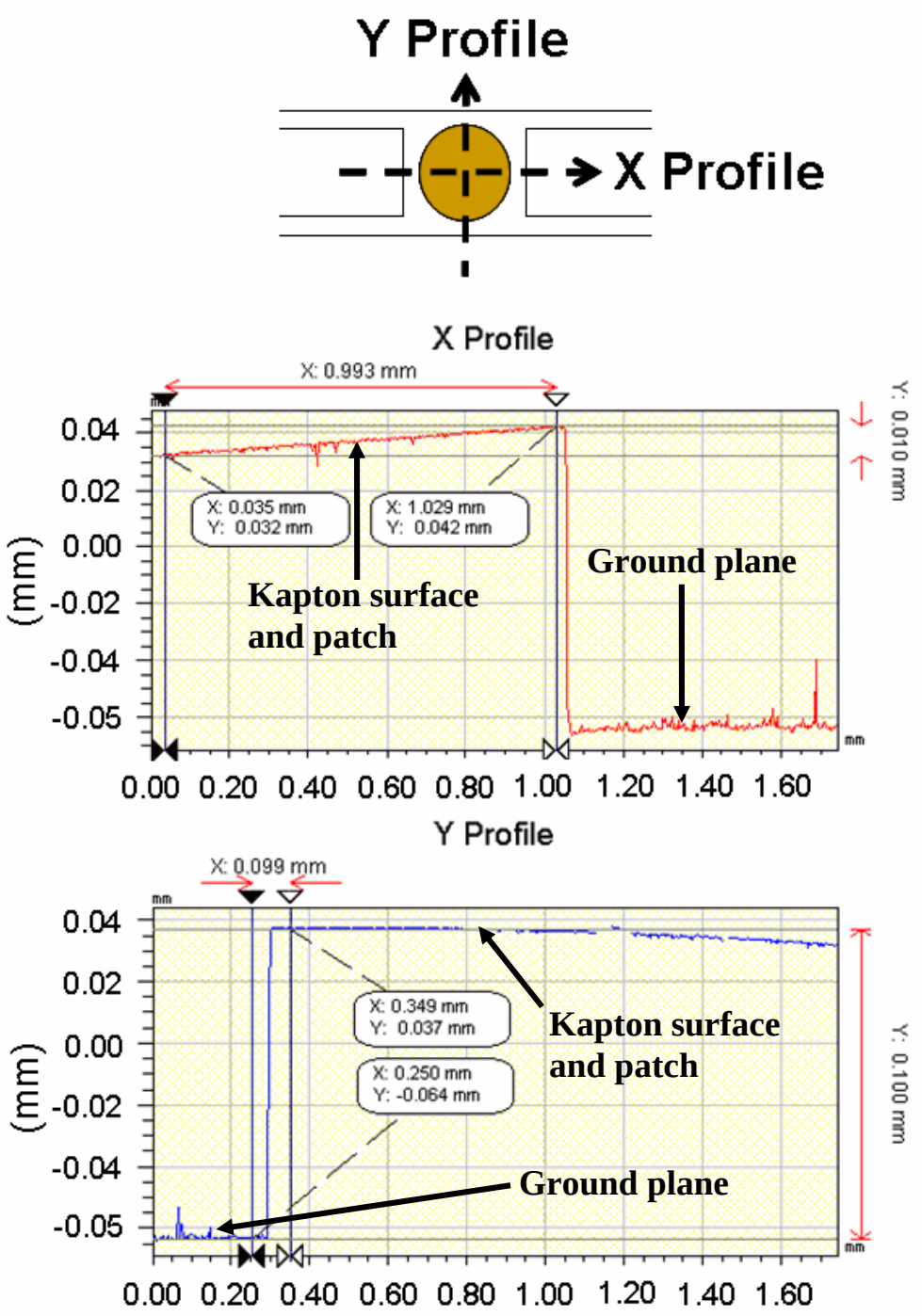

Figure 18: 2D profile of the circular patch antenna measured using WYKO NT 2000 optical profiler.

4.2.2 Return Loss Measurements

The return loss of the MEMS patch antenna was measured using an HP 8510C. Figure 19 shows the setup used for taking return loss measurements on the VNA. A bias tee was connected between the device and the instrument to protect the VNA from possible leakage of high bias voltage. A voltage was applied to the patch and return loss measurements were taken for a range between 0 and 200 V, at 5 or 10 V increments. Figure 20 shows the plot of the return loss measurements on the HP 8510C. The expected downward shift in resonant frequency with increasing bias voltage can be observed. Table 4.1 shows the performance summary of the results shown in Figure 20. At 0 V the antenna is in the "up" state and resonates at 16.91 GHz with a return loss of 59 dB. The antenna is in the "down" state when 165 V is applied and resonates at 16.64 GHz. A steady decrease can be seen throughout the voltage range, averaging near a 10 MHz change per 5 V. The total tunable range was found to be 270 MHz. The return loss is about 59 dB at 16.91 GHz and the bandwidth is about 0.21 GHz for a return loss better than 10 dB. The percentage frequency tuning of the antenna is about 1.6%.

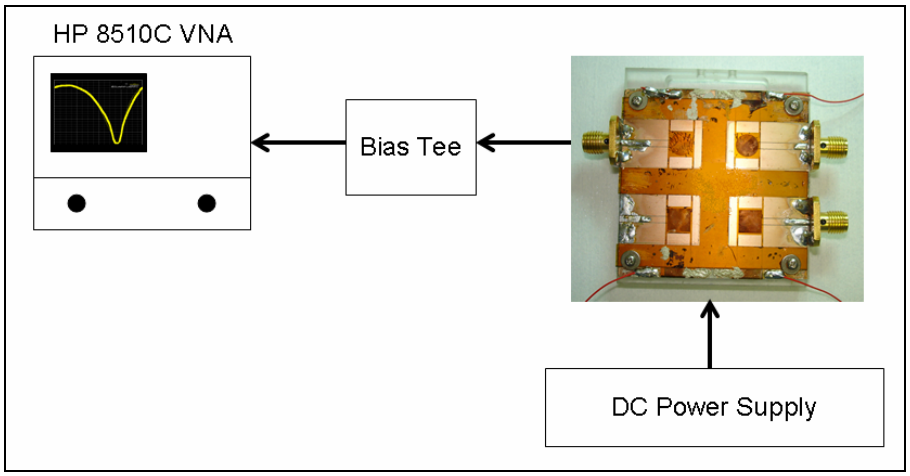

Figure 19: Measurement setup used for testing antenna using the HP 8510C VNA.

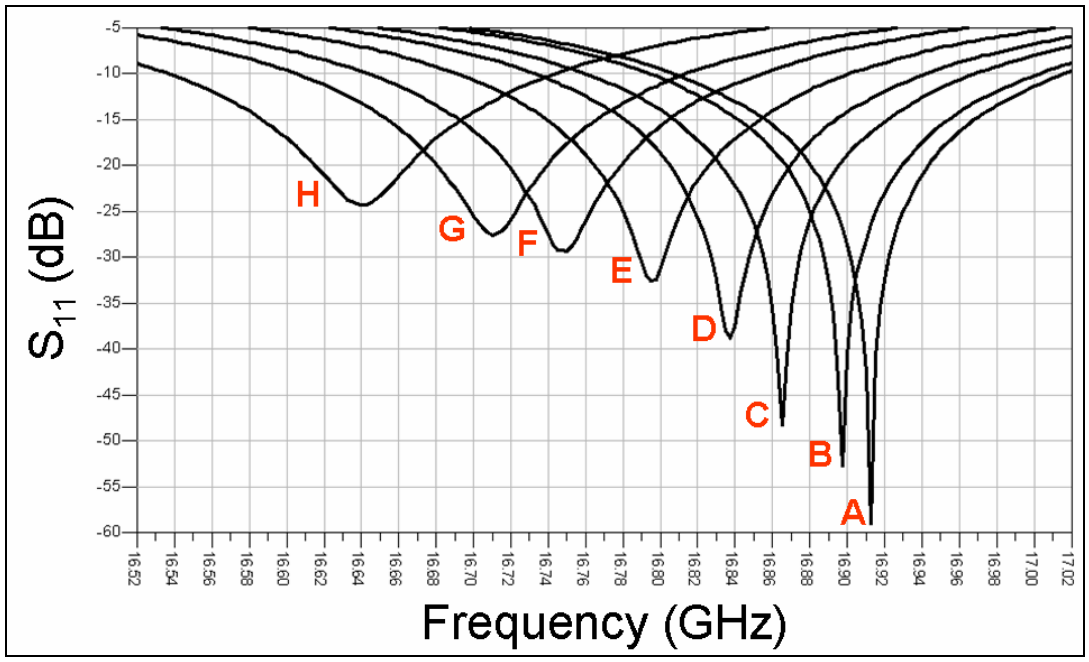

Figure 20: Measured return loss for the circular patch for various applied voltages.

Table 4.1: Performance summary of the MEMS based tunable circular patch antenna for various applied voltages

Plot	*Bias Voltage* (V)	*Resonant Frequency* (GHz)	*Return Loss* (dB)
A	0	16.91	59.077
B	50	16.90	52.859
C	110	16.86	48.339
D	130	16.84	38.737
E	145	16.80	32.614
F	155	16.75	29.270
G	160	16.71	27.586
H	165	16.64	24.258

4.2.3 Radiation Pattern Measurement

A Diamond Engineering 6000 series Desktop Antenna Measurement System (DAMS) was used to measure the radiation patterns. Figure 21 shows a reference for the E and H planes of the circular microstrip design. Measured radiation patterns for various bias voltages V_{dc} = 0, 110, 130, 145, 155, 160 and 165 V, along with the simulated pattern results (up state corresponding to V_{dc} = 0) are shown in Figure 22. It can be noted

that the measured patterns do not change drastically throughout tuning. However, it appears that warpage of the patch has caused tilting of the expected pattern, similar to patterns caused by warpage in the square design. The warped circular patch antenna was modeled in HFSS using parameters from the optical profiler measurements shown in Figure 18. Figure 23 shows the simulated patterns for the warped antenna model. It can be seen that patterns (b), (c), and (d) follow the trend of the warped model, however, the E co polarization pattern does not match. More accurate modeling of the warpage of the circular patch could improve these results.

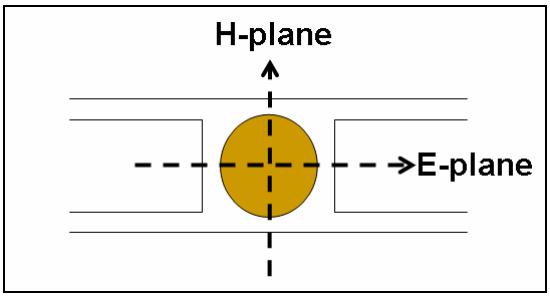

Figure 21: E and H plane of the circular patch antenna.

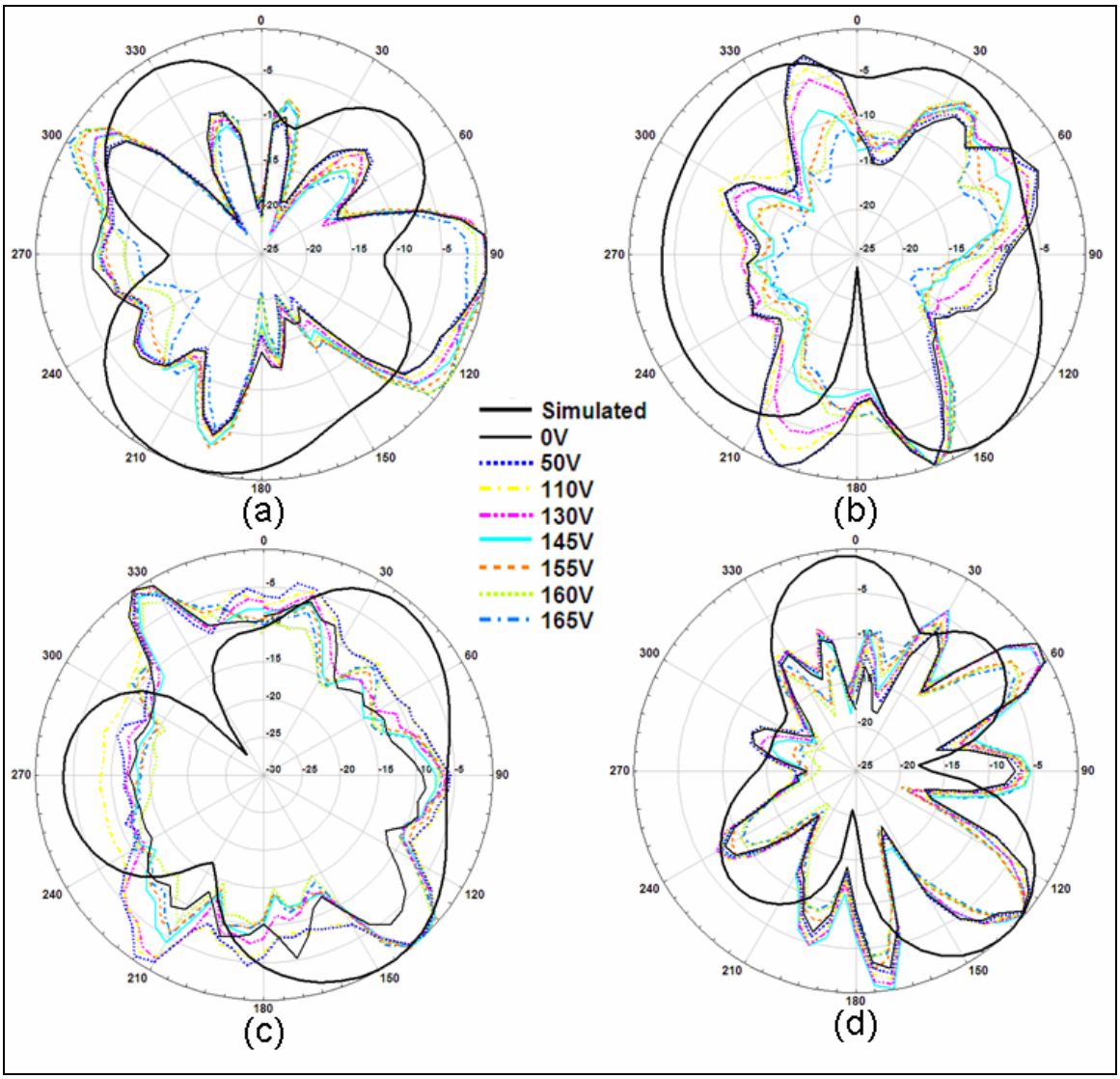

Figure 22: Radiation patterns for circular patch antenna for various applied voltages. (a) E co-polarization (b) E cross polarization (c) H co-polarization (d) H cross polarization.(Note: The simulated pattern is in the up state.)

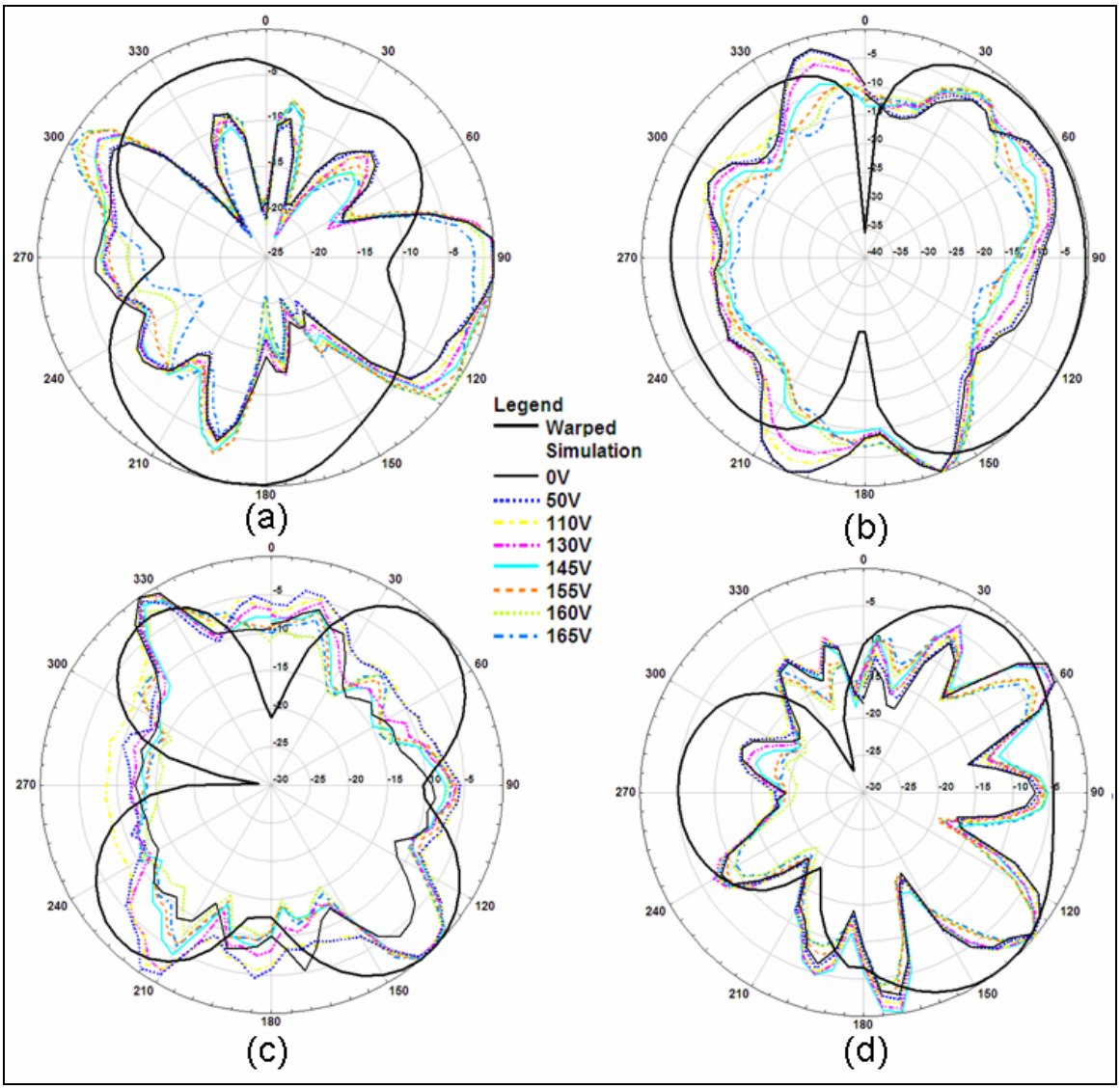

Figure 23: Radiation patterns for circular patch antenna for various applied voltages compared to the simulation results from the warped model in the up state. (a) E co-polarization (b) E cross polarization (c) H co-polarization (d) H cross polarization.

Chapter 5 FABRICATION

One of the major advantages of the tunable microstrip patch antenna is that it is fabricated using proven printed circuit processing techniques such as photolithography, wet etching, and dry etching. Photolithography and wet etching are used to pattern the metallization layer of the substrate, as well as the top side of the kapton. A dry etching process called Deep Reactive Ion Etching (DRIE) is used to cut the kapton film for flexure definition. The Polyflon bonding film is cut such that an air gap is created beneath the patch. This cut can be made either by hand cutting or by a milling machine. The processes used in the fabrication of the substrate and kapton layers can be found in Appendix A.1.

5.1 Material and Setup

The kapton used for the fabrication of the device has a layer of nichrome and a layer of copper deposited on the surface, 100 Å and 2 μm thickness, respectively. The kapton film is mounted, metallization layer up, to a 5 inch silicon wafer for processing. A Dynaflex wafer grip gel is used as an adhesion layer for mounting the kapton film to the wafer. The wafer grip is heated on the wafer to 110°C before placing the kapton film on top. Care is taken to remove any air bubbles from under the kapton before the wafer grip cools. The wafer grip has a two-fold purpose; to hold the kapton film during processing, and to insulate the kapton film from excessive heat during the DRIE process. Rogers

RT/Duroid 6002 is used for the CPW and ground plane of the device. For processing, a 50 *mm* x 50 *mm* square of duroid was placed on a 5 inch silicon wafer with wafer grip for adhesion, just as the kapton film. All processing for fabrication of the MEMS tunable antenna was done in the AMSTC clean room facility in the Electrical Engineering Department at Auburn University. The clean rooms used were a class 10,000 chemical room and class 1,000 photolithography rooms.

5.1.1 Glass Mask Selection

Several glass masks were made with varying over and under sized dimensions. This over and under sizing helped to compensate for over etching in the wet etching process. The CPW mask was made such that all dimensions were 10 microns smaller than called for in the design. 5, 10, 15 and 20 micron under sized masks were considered. The 10 micron mask was found to yield the best dimensions after etching. In similar trials it was found that the 15 micron over sized mask was ideal for definition of the electrodes on the kapton. Because the DRIE dry etching process does not over etch, the exact dimensions were used for that mask.

5.2 Processing

5.2.1 Kapton Top Layer

The kapton film is used as the dielectric insulator for the device and also facilitates actuation of the MEMS device.

5.2.1.1 Photolithography

The term 'Photolithography' refers to the process of defining geometric shapes on the surface of a substrate with the aid of light (typically using Ultraviolet light). The typical steps involved in the photolithographic process are photoresist application, soft baking, mask alignment, exposure and development, and hard-baking [13].

The first step in the fabrication of the kapton top layer is to define "dummy" features of the kapton (shown in Figure 24(a)). This will help in later etching processes, as the total amount of copper that must be etched away is reduced. A positive photoresist, S1813, is spun onto the wafer using a spinner set at 2500 rpm, 500 rps ramp for 30 seconds. After spinning, the photoresist is settled by soft baking at 110°C for 1 minute on a hot plate. Glass masks are used for the exposure process. The wafer is aligned and exposed under a UV lamp with intensity of 7 mW/cm^2 for 15 seconds. Once exposed, the wafer is developed in CD-30 photo developer for 50 seconds. An inspection of the developed photoresist is done under a microscope to ensure uniform development of the features. A hard bake is done at 110°C for 2 minutes on the hot plate.

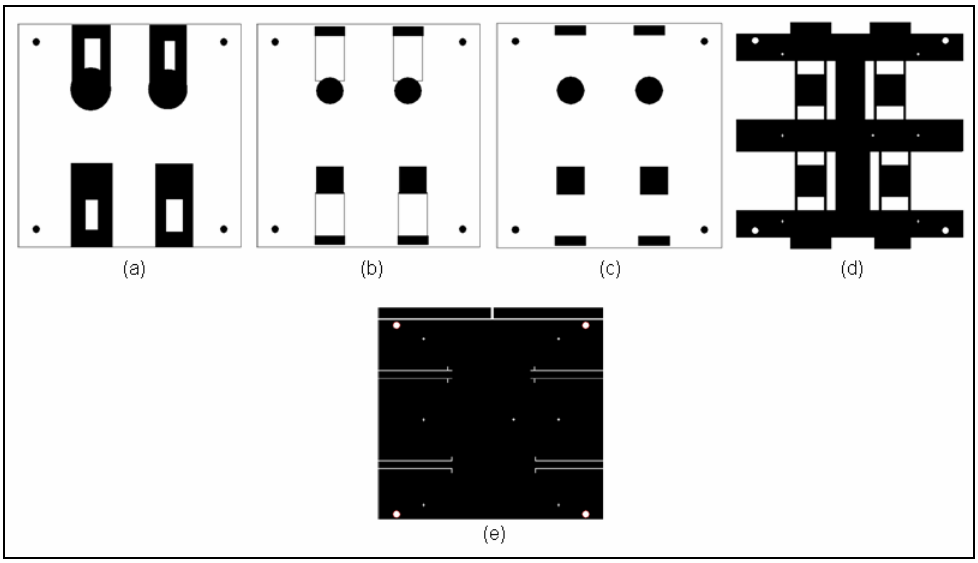

Figure 24: Masks used in photolithography: (a) dummy mask, (b) electrode mask, (c) bias line definition mask, (d) DRIE mask, and (e) CPW mask.

5.2.1.2 Wet Etching

There are two metallization layers that must be etched: copper and nichrome. Etching of the exposed copper is done using Transene CE-200 copper etchant which has an etch rate of 0.5 mil/minute, for an etch time of 7 seconds. A solution of $KMnO_4$ and $NaOH$ is used as nichrome etchant and requires 48 seconds to etch 100 Å thick nichrome layers. It is important to remove any remaining photoresist before submersing in nichrome etchant as it reacts with the nichrome etchant (Appendix A.2.1).

The steps listed in 5.2.1.1 and 5.2.1.2 are repeated for the electrode and bias line definition masks (shown in Figure 24(b), and Figure 24 (c)). Only copper is etched away when defining the bias lines, therefore the nichrome etchant is not used in this step.

5.2.1.3 Deep Reactive Ion Etching

The DRIE dry etching process is used to precisely cut the kapton film. This form of plasma etching is desirable because straight, deep cuts can be made without over

etching. The STS Advanced Oxide Etching (AOE) machine is used with a mixture of 8 sccm CF_4 and 35 sccm O_2 with 500 Watts of RF power. To prevent excessive heating of the kapton, which may cause warpage in the metallization layer due to mismatched thermal expansion, the wafer grip is used to mount the kapton on the silicon wafer. This wafer grip "wicks" away heat from the kapton.

5000 Å of aluminum is deposited via electron beam deposition onto the kapton. The aluminum is used as the masking material for the DRIE process. The same photolithography steps are carried out on the aluminum using the DRIE glass mask (see Figure 24(d)). PAE aluminum etchant is used, for 10 minutes, to define the aluminum DRIE mask. After removing the photoresist, the wafer is placed in the AOE and is processed 5 to 10 minutes at a time for a total of 70 minutes. Once the exposed kapton has been completely removed, a 200 mL solution of 6 grams of $NaOH$ is used to etch away the remaining aluminum (Appendix A.2.2).

5.2.1.4 Probe Station Resistance Measurement

Before the kapton could be laminated onto the substrate, resistance of the bias lines had to be measured to ensure electrical continuity. Bias line resistance of about 18 kΩ was expected. Using a probe station connected to a monitor and multimeter, the resistance of the bias lines was measured. It was found that the bias lines had a resistance of 6 kΩ, less than the expected values, but still within an acceptable range. The less resistance value could be due to over etching of the bias lines.

5.2.1.5 Removal of Kapton Film from Wafer

A bowl of Amyl Acetate is heated to 110°C to dissolve the wafer grip for removal of the kapton film from the silicon wafer. It is important to allow the wafer grip to completely dissolve so that the film does not need to be peeled off the wafer. Peeling the kapton off the wafer will cause warpage of the metallization layer. The removal of the kapton from the wafer grip can take up to 30 minutes.

5.2.2 RT/Duroid Substrate

The fabrication of the CPW feed is done using the same photolithography steps mentioned in section 5.2.1.1. A single mask, the CPW mask (shown in Figure 24(e)), is used to define the feed lines, as well as the electrodes used in biasing the patch on the kapton layer. The RT/Duroid substrate has ¼ oz copper deposited on the surface, this requires 3 minutes and 30 seconds of etch time in CE-200.

5.2.3 Cleaning of Kapton and Substrate

The standard cleaning technique used to remove photoresist and other residue from the kapton film and duroid substrate during processing was liberal rinsing with acetone first, then methanol. Additionally, submersion in a sulfuric acid solution to remove any oxidation on the metallization layers was used. Placement of the film or substrate in a 2% H_2SO_4 bath after each etching and before aluminum deposition ensured that any photo resist spin coat or deposited metal adhered properly to the copper (Appendix A.2.3).

5.2.4 Annealing

As a precaution to reduce the possibility of warpage of the patch antenna, the kapton top layer was annealed before bonding. Annealing was done by placing the fabrication kapton film between two glass plates and heating to 120°C for one hour. The glass plates were placed between two weights to ensure uniform flattening of the kapton. The annealing apparatus was allowed to cool to room temperature before removing the kapton film.

5.2.5 Lamination

The lamination process involves alignment of the three layers followed by thermo-compression bonding. Two stainless steel plates, called bonding jigs, with alignment holes and pins (shown in Figure 25) were used to align the three layers. Alignment holes were created in all three layers (the substrate, bonding film and kapton film) during fabrication described earlier. The sequence of the three layers after alignment is shown in Figure 26. In initial iterations of the design, the bonding process caused warpage of the patch metallization layer. To prevent warpage, kapton strips were placed in the air gap beneath the patch, along with a kapton sheet placed on the kapton top layer with patch (see Figure 26). This sandwiching of the kapton top layer containing the patch antenna helped to reduce warpage during bonding.

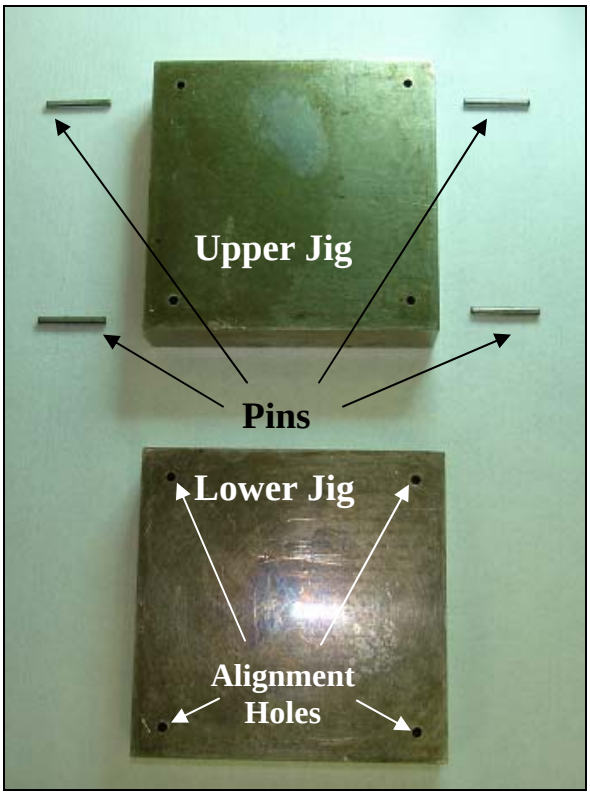

Figure 25: Bonding jig used in lamination.

Thermo-compression bonding was performed using a *Carver Press* consisting of two platens. The platens were heated using heaters, which are controlled by a temperature controller with a thermocouple. The fixture consisting of two steel plates (along with the aligned layers) was placed between the press platens. The bonding was performed at a pressure of 65 psi (a load of 145 lbs.) and a temperature of 130°C. Both pressure and temperature were maintained for 5 minutes during bonding. Before pressure was released, the assembly was allowed to cool down to the room temperature. The fabrication processes employed here are described in [10].

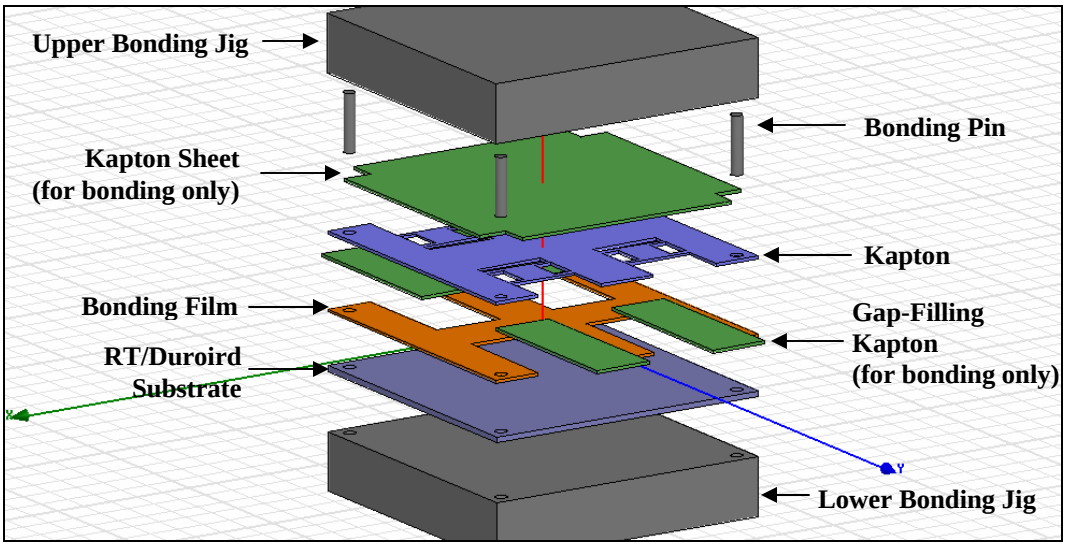

Figure 26: Final sequence of layers for MEMS tunable antenna as on bonding jig.

Chapter 6 CONCLUSION AND FUTURE WORK

6.1 Conclusion

In this work MEMS based tunable square patch and circular patch antennas are presented. A 6 *mm* x 6 *mm* square microstrip patch antenna tunable from 18.34 GHz at 0 V to 17.95 GHz at 268 V and a 6 *mm* diameter circular microstrip patch antenna tunable from 16.91 GHz at 0 V to 16.64 GHz at 165 V have been demonstrated. Both the square and circular patch designs proved to have desirable RF characteristics over the tuning range of 390 MHz and 270 MHz, respectively. In this work, inexpensive tunable antennas fabricated using PCB processing techniques have been demonstrated. These tunable antennas are suitable for implementation of low cost and low profile RF front end, tunable antenna arrays, and tunable reflector arrays.

6.2 Future Work

In both the square and circular patch design, warpage was found to be an issue. In the circular design, warpage was reduced by filling gaps with kapton spacers during bonding. Warpage could further be minimized by fabricating the antenna design discussed in this thesis using liquid crystal polymer (LCP) instead of Kapton polyimide film. The coefficient of thermal expansion of LCP is matched with that of copper (17 ppm) and hence there will be no thermal mismatch between the patch and LCP. In addition, LCP exhibits good dimensional stability, material flexibility, high chemical

resistance, and extremely low moisture absorption, which makes it suitable for the proposed MEMS antenna. An attempt was made, during the research done for this paper, to use a 1 mil LCP film in place of the kapton layer. It was found that the film was too thin to hold a form during the bonding process. Future work on this device should include attempting to use a 2 mil LCP top layer. This may provide for less warpage, lower pull down voltage, and thus better and more efficient tuning.

The MEMS tunable antenna has been constructed here as a stand alone antenna system. Future work may also include integration of the antenna design for array applications. Using this device as a single element in a tunable array or tunable reflector array could be investigated.

REFERENCES

[1] R.R. Garg, P. Bhartia, Inder Bahl, and A. Ittipiboon, Microstrip Antenna Design Handbook, Artech House, Nov. 2000, pp 317 -360.

[2] R. K. F. Lee, K. Y. Ho, J. S. Dahele, Circular-Disk Microstrip Antenna with an Air Gap, IEEE Transactions on Antennas And Propagation, vol. 32, no. 8, Aug. 1984, pp. 880-884.

[3] J. S. Dahele, K. F. Lee, "Theory And Experiment On Microstrip Antennas With Airgaps", *IEE Proceedings*, vol. 132, Pt. H, no. 7, December 1985.

[4] R. V. Goteti, R. Ramadoss, "MEMS-based electrostatically tunable microstrip patch antenna using flexible polyimide film", *Proceedings SPIE* 5798, 198 (2005).

[5] R.V. Goteti, R. E. Jackson, Jr., R. Ramadoss, **"**MEMS-Based Frequency Switchable Microstrip Patch Antenna Fabricated Using Printed Circuit Processing Techniques", *Antennas and Wireless Propagation Letters*, vol. 5, 2006, pp. 228-230.

[6] C. R. Trent, T. M. Weller, "Design and Tolerance Analysis of a 21 GHz CPW-fed Slot-Coupled, Microstrip Antenna on Etched Silicon", *Antennas and Propagation Society International Symposium*, vol. 1, no. 16-21, June 2002, PP.402-405.

[7] Ansoft HFSS version 10.0, Ansoft Corporation, PA, USA.

[8] CoventorWare version 2005.003, Coventor Inc., NC, USA.

[9] Agilent Advanced Design System 2004A, Agilent Technologies, CA, USA.

[10] Ramesh Ramadoss, Simone Lee, Victor M. Bright, Y. C. Lee, and K. C. Gupta, "Polyimide Film Based RF MEMS Capacitive Switches", *IEEE International Microwave Symposium Digest*, Seattle, WA, June 2-7, 2002, pp. 1233-1236.

[11] L. Giauffret and J. M. Laheurte, *Parametric Study of the Coupling Aperture in CPW-Fed Microstrip Antennas*, IEEE Proc-Microw. Antennas Propag., vol 146, no 3, June 1999.

[12] R. Ramadoss and K. C. Gupta, "RF MEMS Devices and Circuit applications", Chapter 14 in I.J. Bahl and P. Bhartia (Eds.), *Microwave Solid State Circuit Design*, John Wiley & Sons, New York, pp. 771-850, Second Edition, April 2003.

[13] A. Sundaram, "Electronically Steerable Antenna Array Using PCB-based MEMS Phase Shifters", Masters Thesis, Auburn University, p. 53, August 2006

Appendix A

A.1 Detailed Fabrication Procedures

CPW Substrate (RT/Duroid 6002)		
1A. Process	Method	Time
2A. Spin coat photoresist	S1813 photoresist	30 seconds 2500 rpm 500 r/s ramp
3A. Soft bake	Hot plate - 110°C	1 minute
4A. UV Exposure	Mask Aligner – expose CPW mask	15 seconds
5A. Develop	CD-30 developer	50 seconds
6A. Hard bake	Hot plate - 110°C	4 minutes
7A. Wet etch	CE-200 etchant	3 minutes
Kapton Film		
1B. Spin coat photoresist	S1813 photoresist	30 seconds 2500 rpm 500 r/s ramp
2B. Soft bake	Hot plate - 110°C	1 minute
3B. UV Exposure	Mask Aligner – expose Electrode definition mask	15 seconds
4B. Develop	CD-30 developer	50 seconds
5B. Hard bake	Hot plate - 110°C	2 minutes
6B. Wet etch Copper	CE-200 etchant	7 seconds
7B. Clean off photoresist	Acetone	-
8B. Wet etch Nichrome	Nichrome etchant	50 seconds
9B. Cleaning	1% H_2SO_4 solution	15 seconds
10B. Repeat steps 1B through 9B for Bias Line Definition mask		
11B. DRIE mask	Deposit 5000 Å Aluminum	
12B. Repeat steps 1B through 5B		
13B. Wet etch Aluminum	PAE Aluminum etchant	10 minutes
14B. DRIE – cut kapton	4:1, CF4 O_2 process	70minutes
15B. Wet etch Aluminum	6g NaOH + 200 mL water	4 minutes

A.2 Chemical Solutions

A.2.1 Nichrome Etchant

DI water	250 mL
$KMnO_4$	10 grams
$NaOH$	5 grams

A.2.2 Post DRIE Aluminum Etchant

DI water	200 mL
$NaOH$	6 grams

Stir for 2 minutes to dissolve $NaOH$

A.2.3 2% Sulfuric Acid Solution

DI water	200 mL
H_2SO_4	2 mL

A.3 Chemical Incompatibilities

The following are notes of chemical incompatibilities that were discovered during the course of fabrication of the MEMS based tunable antennas.

- CE-200 etches aluminum in addition to copper.
- Nichrome reacts with photoresist to create a thick film.
- AZ400K attacks the Nickel in Nichrome.